Int. J. Heat Mass Transfer. Vol. 20, pp. 359–369. Pergamon Press 1977. Printed in Great Britain

THE EFFECT OF SURFACE ROUGHNESS ON THE HEAT TRANSFER FROM A CIRCULAR CYLINDER TO THE CROSS FLOW OF AIR

ELMAR ACHENBACH
Kernforschungsanlage Jülich GmbH, Institut für Reaktorbauelemente, D-5170 Jülich, Postfach 1913, Germany

(*Received* 27 *October* 1975 *and in revised form* 29 *March* 1976)

Abstract—The influence of surface roughness on the heat transfer of a circular cylinder to the cross-flow of air has been studied. The Reynolds number was varied from 2.2×10^4 to 4×10^6. The variation of the roughness parameter was $0 < k_s/d < 900 \times 10^{-5}$. The tests have been performed for the boundary condition $T \approx$ const. For each of the rough cylinders, the static pressure distribution together with the local and total heat transfer have been measured. Particular attention has been paid to the transition from a laminar to a turbulent boundary layer as a function of Reynolds number and roughness parameter.

NOMENCLATURE

a,	constant;
c_p,	specific heat at constant pressure [Ws/kg K];
d,	diameter of the cylinder [m];
D,	pressure drag force [N];
h,	height of the roughness [m];
k_s,	sand grain roughness [m];
l,	length of the cylinder [m];
m,	exponent of the Re-number;
p,	pressure [N/m^2];
s,	pitch of the roughness elements [m];
T,	temperature [K];
U_∞,	undisturbed velocity [m/s].

Greek symbols

α,	heat-transfer coefficient [W/(m^{2}K)];
ε,	emission coefficient;
η,	fluid viscosity [kg/ms];
λ,	heat conductivity [W/mK];
ρ,	fluid density [kg/m^3];
φ,	angular position [degrees].

Subscripts

eff,	effective;
front,	frontal;
g,	gas;
l,	laminar;
t,	turbulent;
tot,	total;
w,	wall;
∞,	undisturbed flow.

Characteristic numbers

c_d	$= D/((\rho/2)U_\infty^2 l \cdot \mathrm{d})$, drag coefficient;
k_s/d,	roughness parameter;
Nu	$= (\alpha d)/\lambda$, Nusselt number;
Pr	$= (\eta c_p)/\lambda$, Prandtl number;
Re	$= (U_\infty d\rho)/\eta$, Reynolds number.

1. INTRODUCTION

IN A PREVIOUS investigation [1] the total and local heat transfer from a smooth circular cylinder in cross flow was examined. The aim was to determine the influence of Reynolds number on the heat transfer, especially in the flow regime around and beyond the critical Reynolds number.

The present investigation accounts for the effect of the surface roughness on the heat transfer. It is well-known from studies of the flow that with increasing roughness parameter, k/d, the critical Reynolds number decreases; this means that at a given point on the surface of the cylinder, the boundary layer undergoes transition from laminar to turbulent flow at decreasing Reynolds numbers [2, 3]. It is, therefore, to be expected that the heat transfer will also be affected by changes in surface roughness.

2. MEASUREMENT TECHNIQUES AND TEST APPARATUS

The preceding investigations of the flow past rough circular cylinders [3] were based on a technique using emery paper as the rough surface. This technique is not appropriate to heat-transfer tests. The present roughness was manufactured by knurling the surface of a copper cylinder. The roughnesses produced by this method were regular arrangements of pyramids, each having a rhomboidal base. The pattern is illustrated in Fig. 1; Table 1 gives the sizes of the three roughnesses tested.

A detailed examination of the geometry of the pyramids exhibited some asymmetries. The height measured from the base lines were different, as can be seen from Table 1 (line 1 and 2) and Fig. 1. The larger roughness heights introduce disturbances from the outer flow into the boundary layer: thus the higher values may be regarded as the effective heights. In line 3 of Table 1 the mean value of the effective height, h_{eff}, is listed; line 4 shows the pitch of the roughness elements; line 5 is referred to below.

Table 1

Height h_I	0.90–0.92	0.40	0.05–0.07 mm
Height h_{II}	0.7	0.47	0.10–0.12 mm
Effective height h_{eff}	0.9	0.45	0.11 mm
Pitch s	2.1	1.2	0.31 mm
k_s/d	900×10^{-5}	300×10^{-5}	75×10^{-5}

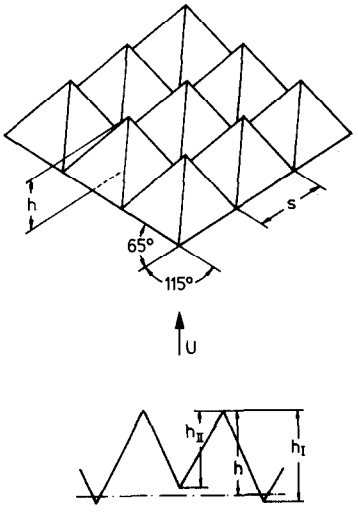

FIG. 1. Roughness pattern.

In principle, the same experimental arrangement and the same measurement techniques were applied as those described in [1]. To facilitate the understanding the salient details are presented in Table 2 and the description is shortly repeated.

The tests were carried out in two wind tunnels of the same internal size. The lower Reynolds number range ($3 \times 10^4 < Re < 3 \times 10^5$) was covered in the atmospheric tunnel, whereas the higher Reynolds numbers ($10^5 < Re < 4 \times 10^6$) were obtained in a high pressure wind tunnel operating with air up to 40 bars.

A sketch of the test section is given in Fig. 2. The cylinder was mounted in a rectangular channel which caused a blockage ratio and span ratio as given in Table 2.

Table 2

1. Test cylinder	
Material	copper
Diameter	0.15 m
Length	0.500 m
Blockage	1:6
Span ratio	3.3
Size of the local probe	$22 \times 3\,mm^2$
2. Wind tunnel	
Working cross-section	$0.5 \times 0.9\,m^2$
Fluid	air at about 30 °C
Pressure	1–40 bars
Temperature difference	9–60 °C
Turbulence level	$Tu = 0.45\%$

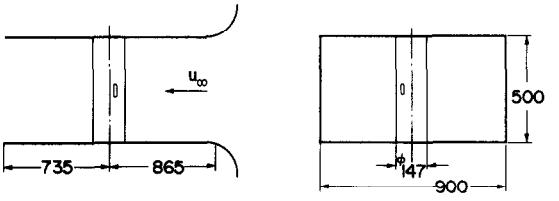

FIG. 2. Sketch of the test section, dimensions in mm.

The copper test cylinder was three-divided. The outer parts acted as guard sections while the center piece represented the active element for the determination of the mean heat-transfer coefficient. The particular sections were thermally insulated from one another and separately heated electrically. Figure 3 represents the design of the test cylinder.

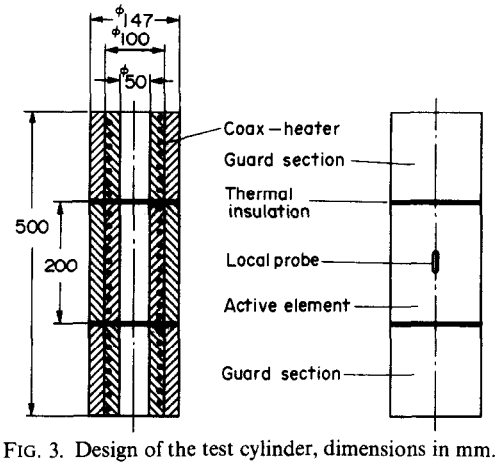

FIG. 3. Design of the test cylinder, dimensions in mm.

The local probe was inserted into the cylinder and flush mounted with the surface. Its dimensions are seen from Fig. 4. The width of 3 mm subtended an angle of about 2.3° at the axis of the cylinder. The probe was also thermally insulated from its surroundings and separately heated at the same temperature within 0.1 K. The cylinder could be rotated around its longitudinal axis. Thus the local distribution of the static pressure and heat transfer was measured by steps of $\Delta\varphi = 5°$.

The tests were intended to be carried out at the boundary conditions $T_{wall} = \text{const}$. For this purpose the cylinder was manufactured from copper which has a high thermal conductivity ($\lambda = 370\,W/mK$). Besides this the cylinder wall was rather thick to compensate for variable circumferential heat flux.

3. RESULTS

3.1. *Local static pressure*

Since there were no data available concerning the effects of pyramidal roughnesses on the flow around circular cylinders, a preliminary study was conducted.

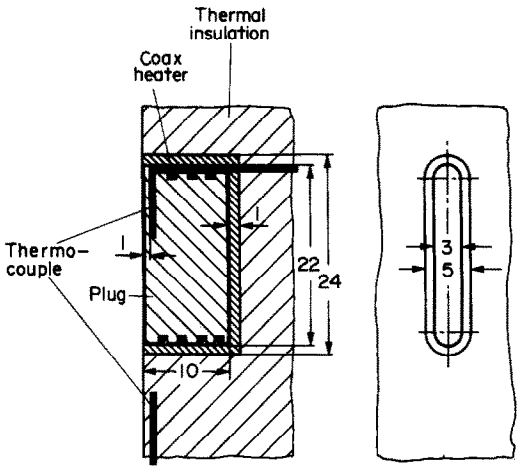

FIG. 4. Design of the local probe, dimensions in mm.

The local static pressure distribution around the circumference of the cylinder was measured as a function of the Reynolds number for each of the three roughnesses. The results are plotted in Figs. 5–7. The local static pressure is plotted against the angle from the front stagnation point, φ, while the Reynolds number appears as a parameter. Additionally, each of the three diagrams shows the pressure distribution according to potential theory. For each roughness parameter the

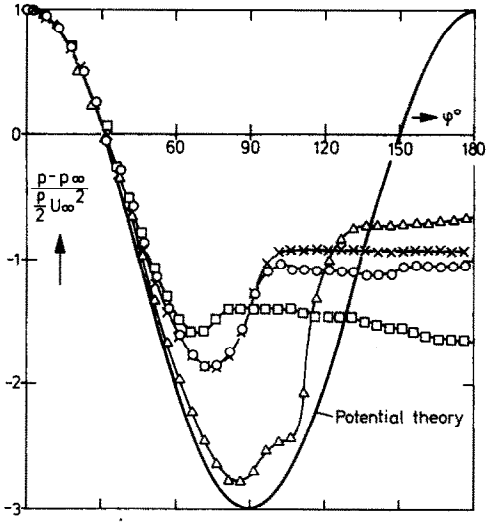

FIG. 5. Local static pressure distribution at $k_s/d = 75 \times 10^{-5}$ and variable Re-number. □, $Re = 8.3 \times 10^4$; △, $Re = 2.2 \times 10^5$; ×, $Re = 5.8 \times 10^5$; ○, $Re = 4.1 \times 10^6$..

Reynolds numbers have been chosen such that the distributions represent the particular flow regimes denoted in Fig. 8 and described below.

For subcritical flow conditions the experimental curve exhibits the most substantial deviations from the theoretical curve. The pressure minimum is located at about $\varphi = 70°$; its value is about $(p-p_\infty)/((\rho/2)U_\infty^2) = -1.5$, compared with -3 for the theoretical distribution. Due to the boundary-layer separation on the front portion of the cylinder, the recovery of the static pressure at the rear is the lowest obtained in the four flow regimes: correspondingly, the drag coefficient takes its highest values (see Fig. 10).

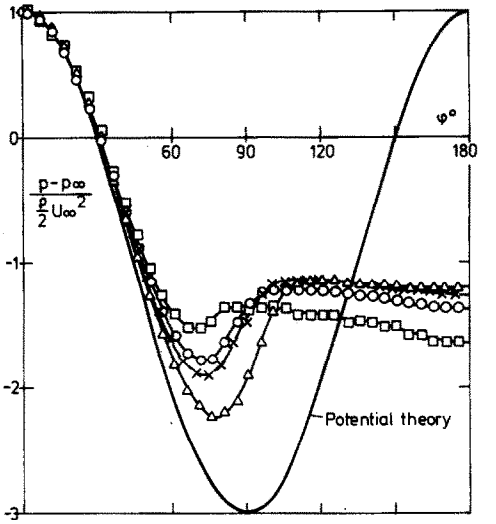

FIG. 6. Local static pressure distribution at $k_s/d = 300 \times 10^{-5}$ and variable Re-number. □, $Re = 6.3 \times 10^4$; △, $Re = 1.16 \times 10^5$; ○, $Re = 1.38 \times 10^5$; ×, $Re = 4 \times 10^6$.

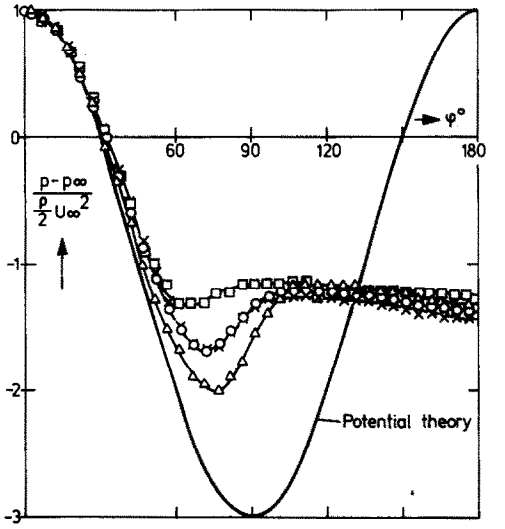

FIG. 7. Local static pressure distribution at $k_s/d = 900 \times 10^{-5}$ and variable Re-number. □, $Re = 5 \times 10^4$; △, $Re = 6.1 \times 10^4$; ×, $Re = 3.8 \times 10^5$; ○, $Re = 4 \times 10^6$.

Under critical flow conditions the experimental pressure distribution comes close to that of the theoretical curve. In particular, the pressure gain in the rear is substantial so that the drag coefficient is low. This effect results from the shifting of the boundary layer separation point downstream to $\varphi = 140°$, i.e. the flow follows the contour of the cylinder up to this position.

The pressure distributions for the supercritical and transcritical flow ranges fall between those of the critical and subcritical flow ranges, and provide intermediate values for the drag coefficient.

The pressure distributions measured for the four flow ranges are qualitatively the same for each of the three roughness conditions. However, it is obvious that with increasing roughness parameter the value of the minimum static pressure decreases. This is in good agreement with the fact that the drag coefficient at Re_{crit} increases with increasing roughness parameter.

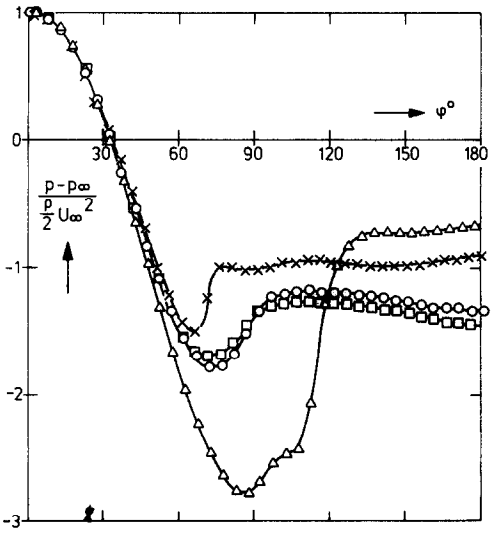

FIG. 8. Local static pressure distribution at $Re = 2.2 \times 10^5$ and variable roughness parameter. ×, smooth; △, $k_s/d = 75 \times 10^{-5}$; ○, $k_s/d = 300 \times 10^{-5}$; □, $k_s/d = 900 \times 10^{-5}$.

Figures 8 and 9 represent the pressure distribution at a constant Reynolds number for variable roughness parameter. At $Re = 2.2 \times 10^5$ (Fig. 8) the flow is just passing from the subcritical to the critical state for the smooth cylinder. It is critical for the smallest roughness parameter $k_s/d = 75 \times 10^{-5}$, nearly transcritical for $k_s/d = 300 \times 10^{-5}$ and completely transcritical for $k_s/d = 900 \times 10^{-5}$. The pressure distributions indicate that the drag coefficients at $Re = 2.2 \times 10^5$ decrease in the sequence of the roughness parameters $k_s/d = 900 \times 10^{-5}$, $k_s/d = 300 \times 10^{-5}$, $k_s/d = 75 \times 10^{-5}$ (see also Fig. 10). In Fig. 9 the distribution of the static pressure is plotted for $Re = 4 \times 10^6$: the flow is transcritical for each of the four roughness conditions. From the local pressure it can be seen that with increasing roughness parameter the drag coefficient increases.

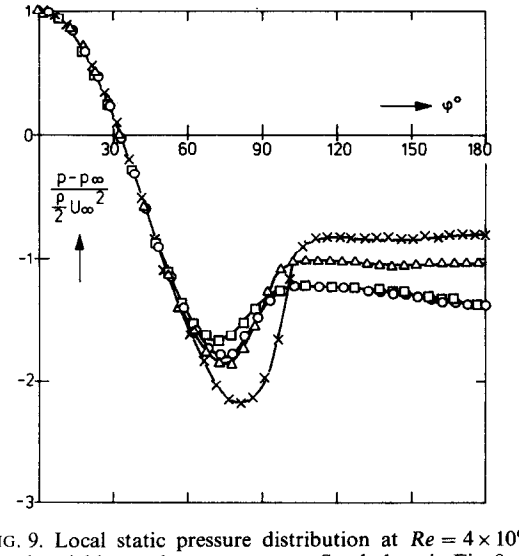

FIG. 9. Local static pressure distribution at $Re = 4 \times 10^6$ and variable roughness parameter. Symbols as in Fig. 8.

Moreover, it is evident that the pressure distributions measured for the two highest roughnesses are very similar which leads to identical values of the drag coefficient. This phenomenon is discussed in conjunction with Fig. 10 below.

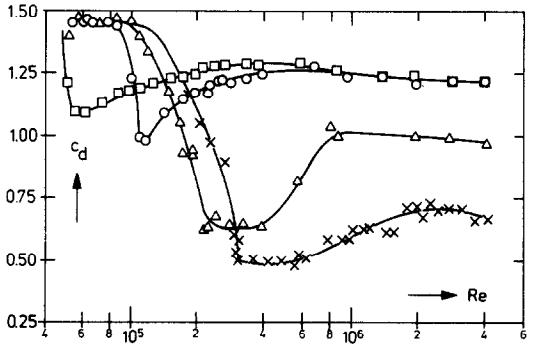

FIG. 10. Pressure drag coefficient as a function of Re and roughness parameter k_s/d. Symbols as in Fig. 8.

3.2. *Drag coefficient*

The integration of the local pressure around the circumference of the cylinder yields the pressure drag coefficient, c_d. It is defined as

$$c_d = \frac{D}{\frac{\rho}{2} U_\infty^2 \, d \cdot 1}.$$

According to the results of Achenbach [3] the total drag, which includes the effects of skin friction forces, can be estimated to be about 0.5–2% higher—depending on Reynolds number—than the pressure drag. In Fig. 10 the pressure drag coefficient has been plotted as a function of the Reynolds number.

It is evident that the roughness parameter k_s/d affects the flow past the cylinder since there is a different curve for each value of the roughness parameter. In essence, the experimental curves have a shape as illustrated in Fig. 11. Four flow ranges can be distinguished, which are characterized by the boundary layer phenomena described in [1] and [3].

For subcritical flow conditions the boundary layer separates laminarly at an angular position $\varphi = 82°$. The drag coefficient is nearly independent of the Reynolds number.

In the critical flow range the drag coefficient drops rapidly with Reynolds number because the separation point moves downstream. At first the boundary layer still separates laminarly. However, when the angle of

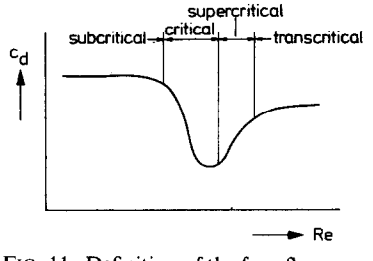

FIG. 11. Definition of the four flow ranges.

laminar boundary layer, $\varphi = 110°$, is reached the flow changes substantially. The boundary layer laminarly separates at $\varphi = 110°$ and forms a free shear layer, which immediately downstream experiences a transition to turbulent flow. Finally the free shear layer reattaches turbulently to the wall as a turbulent boundary layer. This phenomenon is known in the literature as the occurence of separation bubbles. The separation point shifts downstream to $\varphi = 140°$ and causes a considerable gain of the static pressure in the rear, which leads to low drag forces. The Reynolds number where the drag coefficient exhibits a minimum is termed the "critical Reynolds number", Re_{crit}.

In the supercritical flow range the drag coefficient rises again. The separation bubbles exist no longer. There is a direct transition from a laminar to a turbulent boundary layer at a position some degrees downstream of the maximum cross-section. With increasing Reynolds number the position of boundary layer separation moves upstream causing the drag coefficient to increase.

Under transcritical flow conditions the laminar–turbulent transition takes place on the front portion of the cylinder. Its exact position depends on the Reynolds number as well as on the roughness parameter: this is discussed below in connexion with the local heat-transfer coefficient. The position of the separation point is nearly independent of the Reynolds number so that the drag coefficient is also constant.

From Fig. 10 it can be seen that with increasing roughness parameter the critical Reynolds number decreases. This result is plausible since, with decreasing Reynolds number, the boundary layer thickens so that the roughness is gradually submerged in it. Thus the disturbances put into the boundary layer from regions of high velocity diminish until they are so small that they are damped out without causing transition to turbulence. The consequence of this should be a collapse of all experimental curves in the subcritical flow regime. Figure 10 demonstrates that this is indeed the case.

Furthermore, it should be mentioned that for the higher roughnesses the flow range where the separation bubbles occur shrinks to a single point, which is at the same time the critical Reynolds number. This phenomenon was also observed in [3].

In the transcritical flow regime the drag coefficient increases with increasing roughness parameter, as mentioned above. However, it appears that an upper limit exists such that, if the roughness parameter is increased beyond a certain value, no increase in drag coefficient occurs. A similar observation has been made for the flow past rough spheres [4]. The reason may be that the roughness heights become large compared with the thickness of the boundary layer. Thus the top of a roughness element does not protrude into regions of higher velocities if the roughness height is increased. This hypothesis would agree with the observations made concerning the total heat transfer which, as demonstrated below in Fig. 18, also seems to exhibit an upper limit.

The drag coefficient results reported in [3] and the present ones are observed to differ from one another. This seems to be due to the different kinds of surface roughness. While the pyramidal roughness is a regular arrangement of roughness elements the roughness of the emery paper has a more random character.

3.3. *Classification of the roughness*

For the classification of the roughnesses in terms of the sand grain roughness, k_s/d, the results were compared with those reported in [2]. The criterion applied was the magnitude of the critical Reynolds number since it depends on the surface roughness. Of course, this criterion is not entirely convincing, as the flow conditions also depend on the roughness pattern. However, the criterion chosen represents the best that was available to the author at the time. Figure 12 illustrates the evaluation of the criterion. The critical

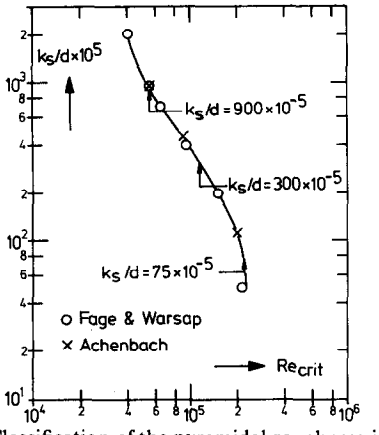

FIG. 12. Classification of the pyramidal roughness in terms of sand grain roughness after Fage and Warsap [2] and Achenbach [3].

Reynolds number was determined experimentally for each of the three pyramidal roughnesses. The following results were obtained:

$$Re_{crit} = 2.1 \times 10^5, \quad k_s/d = 75 \times 10^{-5}$$

$$Re_{crit} = 1.15 \times 10^5, \quad k_s/d = 300 \times 10^{-5}$$

$$Re_{crit} = 5.7 \times 10^4, \quad k_s/d = 900 \times 10^{-5}.$$

These values have also been listed in line 5 of Table 1.

The roughness parameter of the smallest roughness could not be determined with great accuracy. As demonstrated by Fig. 12 the curve is very steep and its course is rather uncertain in this Reynolds number range.

3.4. *Local heat transfer*

The local heat-transfer coefficient was measured by means of a thermally insulated plug inserted into the surface of the cylinder. This method and the experimental difficulties resulting from it have been described previously [1] and are therefore not repeated herein.

In Figs. 13–15 the local heat-transfer distribution around the cylinder is plotted for each of the three roughnesses tested. The parameter varied is the

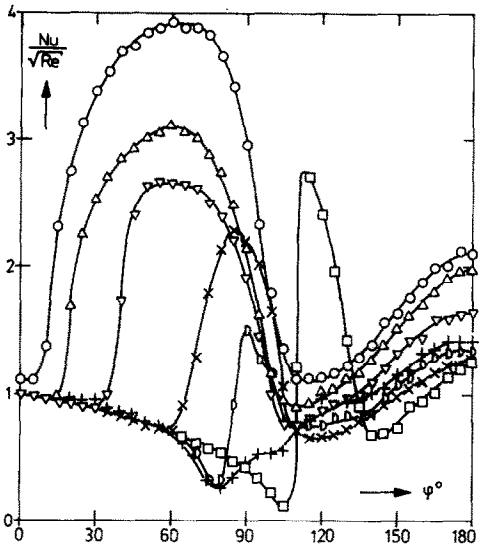

FIG. 13. Local heat-transfer coefficient at $k_s/d = 75 \times 10^{-5}$ and variable Re-number, $Pr = 0.72$. +, $Re = 9.2 \times 10^4$; ○, $Re = 1.9 \times 10^5$; □, $Re = 4.1 \times 10^5$; ×, $Re = 5.9 \times 10^5$; ▽, $Re = 9.0 \times 10^5$; △, $Re = 1.9 \times 10^6$; ○, $Re = 4.0 \times 10^6$.

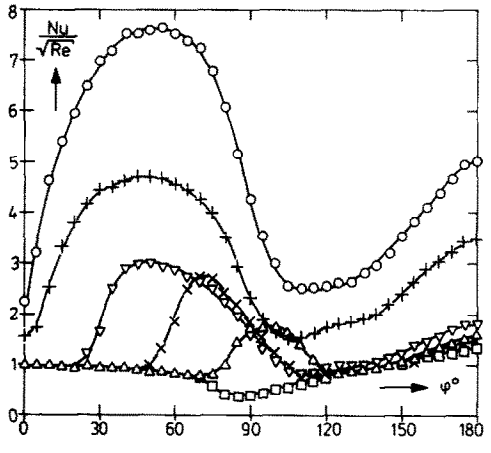

FIG. 14. Local heat-transfer coefficient at $k_s/d = 300 \times 10^{-5}$ and variable Re-number, $Pr = 0.72$. □, $Re = 7.2 \times 10^4$; △, $Re = 1.27 \times 10^5$; ×, $Re = 1.46 \times 10^5$; ▽, $Re \times 2.26 \times 10^5$; +, $Re = 8.6 \times 10^5$; ○, $Re = 4 \times 10^6$.

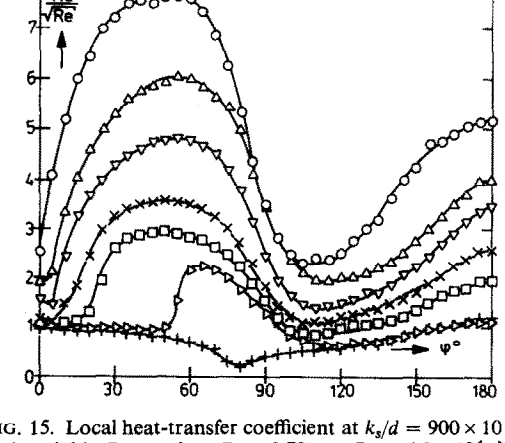

FIG. 15. Local heat-transfer coefficient at $k_s/d = 900 \times 10^{-5}$ and variable Re-number, $Pr = 0.72$. +, $Re = 4.8 \times 10^4$; ▷, $Re = 7.3 \times 10^4$; □, $Re = 2.8 \times 10^5$; ×, $Re = 3.8 \times 10^5$; ▽, $Re = 8.8 \times 10^5$; △, $Re = 1.9 \times 10^6$; ○, $Re = 4.1 \times 10^6$.

Reynolds number. The Nusselt number is normalized by $Re^{-0.5}$. This presentation is appropriate in the presence of laminar boundary layers, as can be seen from the heat transfer near the stagnation point where the curves collapse for all Reynolds numbers (see for instance Fig. 13). Where a turbulent boundary layer exists the peak values of the curves increase with increasing Reynolds number. Further analysis of the experimental results show that the peak values increase as approximately Re^m ($0.8 < m < 0.85$). The same trend is found also for the heat transfer in the rear of the cylinder where separated flow occurs. Thus the local heat transfer already indicates that the total heat-transfer coefficient will also increase in the transcritical flow range, depending on Re^m ($0.8 < m < 0.85$).

Figure 13 shows the results for the smallest roughness ($k_s/d = 75 \times 10^{-5}$). Each of the four flow ranges is represented. In the subcritical range ($Re = 9.2 \times 10^4$) the boundary layer is laminar throughout; its separation is indicated by the minimum near $\varphi = 80°$. The heat-transfer distribution in the critical flow range ($Re = 4.1 \times 10^5$) is characterized by the occurrence of separation bubbles, located at the minimum of Nu near $\varphi = 105°$, as well as by the substantial rise of Nu in the region where the turbulent shear layer reattaches to the wall, causing very high values of the heat-transfer coefficient. At about $\varphi = 140°$ the turbulent boundary layer separates as indicated by another minimum in the experimental curve. The curve $Re = 5.9 \times 10^5$ represents the supercritical flow range. There is a direct transition from a laminar to a turbulent boundary layer at $\varphi = 60°$, generating high heat-transfer coefficients downstream. The separation occurs around $\varphi = 115°$.

With further increase of the Reynolds number, the laminar–turbulent transition point approaches the front stagnation point. At about $Re = 10^6$ the transcritical flow range is reached, characterized by the presence of a turbulent boundary layer on the entire cylinder surface upstream of the separation point—except in the immediate vicinity of the front stagnation point.

Figures 14 and 15 qualitatively show similar results for the local heat transfer with the remaining two roughnesses. The essential difference is that, with increasing roughness parameter, the transition from a laminar to a turbulent boundary layer, considered for a fixed position, occurs at a decreasing Reynolds number. This point is particularly clear in Figs. 16 and 17, which represent the local heat transfer at a constant Reynolds number for the roughnesses tested.

The heat-transfer results at the front stagnation point would be expected to be equal to unity, as the flow near the stagnation point is laminar and as the turbulence level is low ($Tu = 0.45\%$). However, Figs. 14 and 15 indicate that, for the highest Reynolds numbers, their values are greater than unity. This effect is due to the finite width of the local probe (3 mm) as well as to the circumferential heat flux caused by the considerable increase of the heat-transfer coefficient with increasing angle from the front stagnation point.

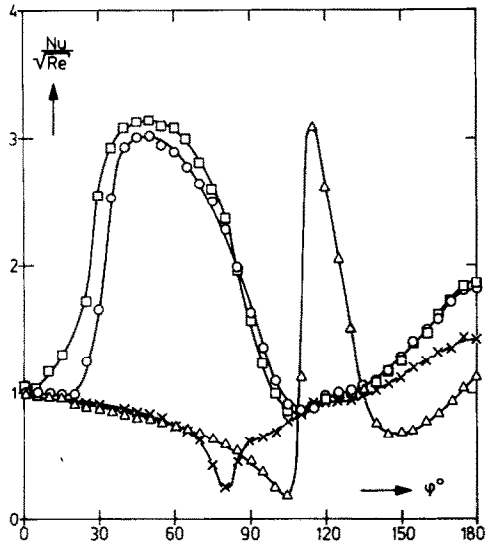

FIG. 16. Local heat-transfer coefficient at $Re = 2.2 \times 10^5$ and variable roughness parameter, $Pr = 0.72$. Symbols as in Fig. 8.

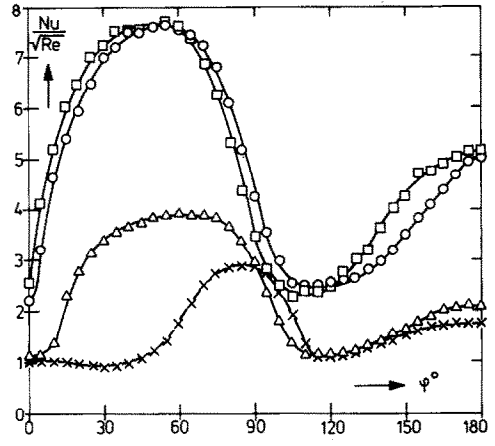

FIG. 17. Local heat-transfer coefficient at $Re = 4 \times 10^6$ and variable roughness parameter, $Pr = 0.72$. Symbols as in Fig. 8.

Figures 16 and 17 may be compared with those illustrating the local static pressure distribution around the rough cylinder (Figs. 8 and 9). At $Re = 2.2 \times 10^5$ the flow past the smooth cylinder is still subcritical. However, the smallest roughness just causes critical flow conditions: the phenomenon of the separation bubble associated with the substantial increase of the heat-transfer coefficient is apparent. Transcritical flow conditions are found for the cylinders covered with the two greatest roughnesses. The highest roughness causes laminar–turbulent transition at about 5° further upstream compared with the next lower roughness. At $Re = 4 \times 10^6$ the transition from a laminar to a turbulent boundary layer takes place on the front portion of the cylinder for each of the four surface roughnesses. Except in the case of the smooth cylinder, transition occurs at $\varphi < 5°$. Furthermore, Fig. 14 reveals that the cylinders covered with the roughnesses $k_s/d = 900 \times 10^{-5}$ and $k_s/d = 300 \times 10^{-5}$ have the same value of the total heat-transfer coefficient, as shown in Fig. 18.

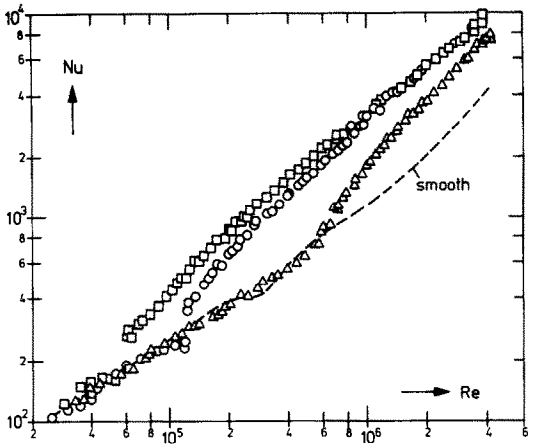

FIG. 18. Total heat-transfer coefficient as a function of Re and roughness parameter k_s/d, $Pr = 0.72$. Symbols as in Fig. 8; _ _ _ _ smooth after Achenbach [1].

3.5. *Total heat transfer*

The total heat-transfer coefficient is presented as a function of the Reynolds number in Fig. 18. The parameter varied is the surface roughness, expressed in terms of k_s/d. Under subcritical flow conditions the four curves collapse, as expected from the relationship between pressure drag coefficient and Reynolds number. The curves separate in terms of k_s/d when the critical Reynolds number is reached. This is why the heat transfer gradually increases since the transition point from a laminar to a turbulent boundary layer moves upstream. During this phase the slope, m, in the relationship $Nu = aRe^m$ is about unity or higher. The slope gradually decreases to $m \approx 0.8$, when the transition occurs in the immediate vicinity of the stagnation point, i.e. if the whole boundary layer is turbulent.

In the transcritical flow range, surface roughening increases the heat transfer by a factor of approximately 2.5. As mentioned above, the curves representing the results for the two largest roughnesses collapse in the transcritical flow range. This effect has already been discussed in connexion with the results of the drag coefficient.

The Figs. 19–21 have been separated to show the details of the curves in the critical and supercritical flow range; it may be demonstrated that a simple relationship of the form $Nu = aRe^m$ cannot be applied in the range covered by the present experiments. At subcritical flow conditions the heat-transfer coefficient can be described by a 0.63-power of the Reynolds number for the three roughness conditions. Equation (1) describes the heat transfer as a function of Re at subcritical flow conditions for $Re > 10^4$ and $Pr = 0.72$

$$Nu = 0.18\, Re^{0.63}. \tag{1}$$

In the range where the drag coefficient falls rapidly (see Fig. 10) the Nusselt number becomes independent of the Reynolds number. This can be explained by the extension of the laminar boundary layer in the Reynolds number range immediately preceding the critical Reynolds number. Thus a large portion of the cylinder surface is covered with a laminar boundary

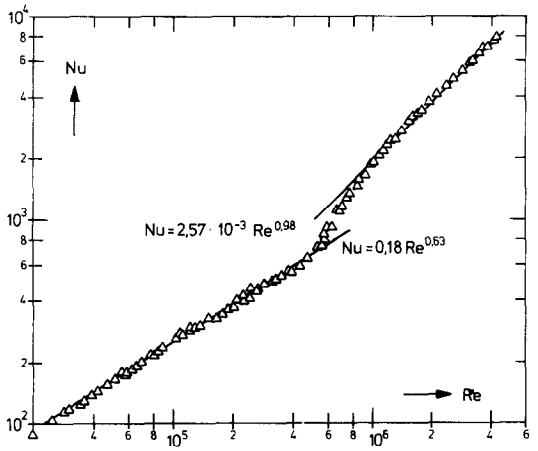

FIG. 19. Total heat-transfer coefficient for $k_s/d = 75 \times 10^{-5}$, $Pr = 0.72$.

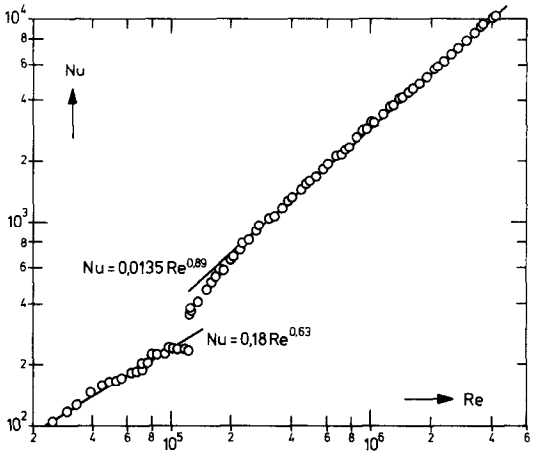

FIG. 20. Total heat-transfer coefficient for $k_s/d = 300 \times 10^{-5}$, $Pr = 0.72$.

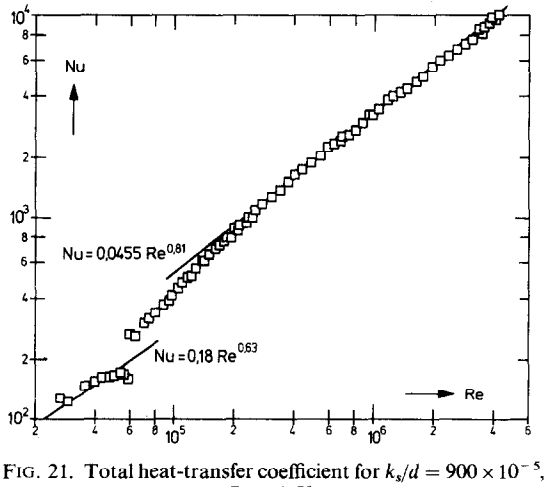

FIG. 21. Total heat-transfer coefficient for $k_s/d = 900 \times 10^{-5}$, $Pr = 0.72$.

layer which represents a considerable heat resistance. At the critical Reynolds number the rapid increase of the local heat-transfer coefficient occurs due to the transition to a turbulent boundary layer near the main cross-section of the cylinder. This gives rise to a stepwise increase in the total heat-transfer coefficient. For high roughness parameters the critical flow range barely extends beyond the critical Reynolds number in contrast to the results for the smooth cylinder or the lowest roughness parameter $k_s/d = 75 \times 10^{-5}$. As indicated in Fig. 10, the drag coefficient for the two largest roughness parameters begins to increase immediately when the critical Reynolds number is exceeded, and it is this increase that characterizes the supercritical Reynolds number range. While, in the supercritical flow range, the length of the turbulent boundary layer gradually increases due to the upstream shifting of the transition point, the total Nusselt number also increases. As demonstrated below in Fig. 27, the upstream shifting of the transition point occurs in a rather narrow Reynolds number range. This results in a considerable increase of the total heat transfer in this range. Expressed in terms of the slope in the relationship $Nu = aRe^m$, the increase is so substantial that m becomes greater unity.

At the Reynolds number where the drag coefficient reaches a new plateau (transcritical flow), the Nusselt number also levels out to obey the simple relationship. $Nu = aRe^m$, at least over a restricted range. However, the exponent m is not the same for each of the roughnesses. The tests have shown that m decreases with increasing roughness. The following relationships are obtained from the experiments.

Smooth cylinder:

$$Nu = 9.02 \times 10^{-4} Re^{1.01}; \tag{2}$$

Range of validity:

$$Pr = 0.72, \quad 1.5 \times 10^6 < Re < 4 \times 10^6.$$

Rough cylinder:

$$k_s/d = 75 \times 10^{-5}$$
$$Nu = 2.57 \times 10^{-3} Re^{0.98}; \tag{3}$$

Range of validity:

$$Pr = 0.72, \quad 10^6 < Re < 4 \times 10^6.$$

Rough cylinder:

$$k_s/d = 300 \times 10^{-5}$$
$$Nu = 0.0135\, Re^{0.89}; \tag{4}$$

Range of validity:

$$Pr = 0.72, \quad 3 \times 10^5 < Re < 4 \times 10^6.$$

Rough cylinder:

$$k_s/d = 900 \times 10^{-5}$$
$$Nu = 0.0455\, Re^{0.81}; \tag{5}$$

Range of validity:

$$Pr = 0.72, \quad 3 \times 10^5 < Re < 4 \times 10^6.$$

In Fig. 22 the heat-transfer results of Daujotas *et al.* [5] are compared with the present ones for the smooth cylinder. Under subcritical conditions the values of Daujotas *et al.* are about 10% lower; for critical conditions the difference increases to about +30%. In the supercritical and transcritical flow range deviations lower than 10% are observed. The differences between the results may be caused by the different boundary conditions in the two tests, i.e. Daujotas *et al.* used a

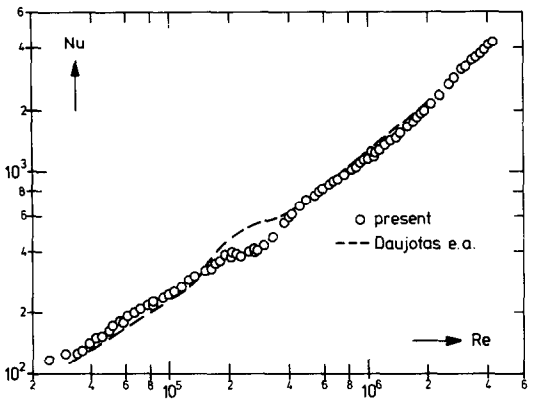

FIG. 22. Total heat transfer for smooth cylinder. Comparison with the results of Daujotas *et al.* [5].

nearly constant heat flux whereas our results were carried out at nearly constant surface temperature. Moreover, the reference temperature at which the properties were evaluated may affect the comparison. The properties of the fluid in the present tests were evaluated at the outer gas temperature, except for the heat conductivity λ. T_λ was chosen as

$$T_\lambda = T_w - \tfrac{1}{4}(T_w - T_g).$$

The third effect which may have influenced the results is the surface condition: as Daujotas *et al.* used cylinders with a maximum diameter of 50 mm, the surface roughness may have affected the results. Finally the blockage ratio at high Reynolds numbers was larger than that of the present investigation (1:3.6, present 1:6).

3.6. *Further evaluation of the local heat-transfer results*

The evaluation of the local heat-transfer results yields the percentage contribution of the heat transferred at the front part of the cylinder to the total heat. Figure 23 presents the results for the three roughnesses, together with those for the smooth cylinder [1]. At subcritical flow conditions, Nu_{front} decreases with increasing Reynolds number since the heat transfer in the rear of the cylinder gradually increases. Beyond the critical Reynolds number the peak values of heat transfer due to the transition to a turbulent boundary layer cause a further decrease of Nu_{front}. As the transition point moves upstream in the supercritical flow range, the heat transfer increases over the front part of the cylinder, leading to a rise in Nu_{front}. In the transcritical flow range, which is characterized by a predominantly turbulent boundary layer, the ratio of Nu_{front}/Nu_{tot} becomes independent of the Reynolds number. Moreover, the value levels out for all roughness conditions to $Nu_{front}/Nu_{tot} = 0.62$.

From Figs. 24–26 the rate of heat transfer either through a laminar boundary layer (Nu_l) or a turbulent boundary layer (Nu_t) or a separated flow region (Nu_s) can be seen for each of the roughness conditions. Under subcritical flow conditions the heat is transferred in nearly equal proportions through the laminar boundary layer and the separated flow region. The experiments demonstrate that, with decreasing Reynolds number, the percentage contribution of the laminar boundary-layer heat transfer increases. Once beyond the critical Reynolds number the contribution from the turbulent boundary layer can also be considered. Since the length of the turbulent boundary

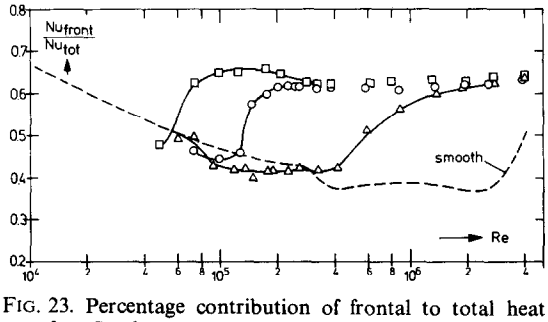

FIG. 23. Percentage contribution of frontal to total heat transfer. Symbols as in Fig. 8, ——— smooth after Achenbach [1].

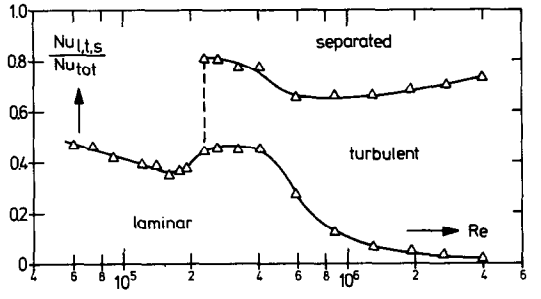

FIG. 24. Percentage contribution of laminar, turbulent and separated flow heat transfer to total heat transfer at $k_s/d = 75 \times 10^{-5}$

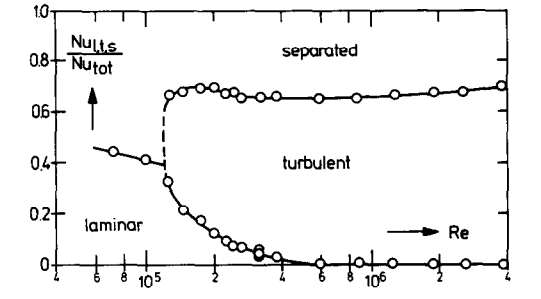

FIG. 25. Percentage contribution of laminar, turbulent and separated flow heat transfer to total heat transfer at $k_s/d = 300 \times 10^{-5}$.

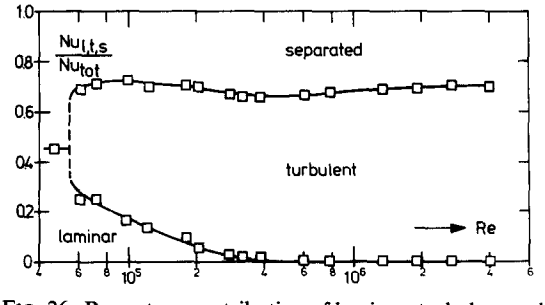

FIG. 26. Percentage contribution of laminar, turbulent and separated flow heat transfer to total heat transfer at $k_s/d = 900 \times 10^{-5}$.

layer increases with increasing Reynolds number, the rate Nu_t increases at the cost of Nu_l, which finally approaches zero. In the transcritical flow range the heat transfer is maintained predominantly through the turbulent boundary layer (70%), only 30% passing through the separated flow region. Whereas the curves representing the results for the two highest roughnesses are quite similar, the curve referring to the lowest roughness parameter is somewhat different since the critical flow range extends beyond the critical Reynolds number. It is evident that this curve is similar to that for the smooth cylinder [1] since the flow conditions of the critical flow range are also similar.

The rapid increase of the local heat-transfer coefficient indicates the transition from a laminar to a turbulent boundary layer. Thus the position of boundary-layer transition can be obtained from the heat transfer results. Figure 27 represents the angle of transition,

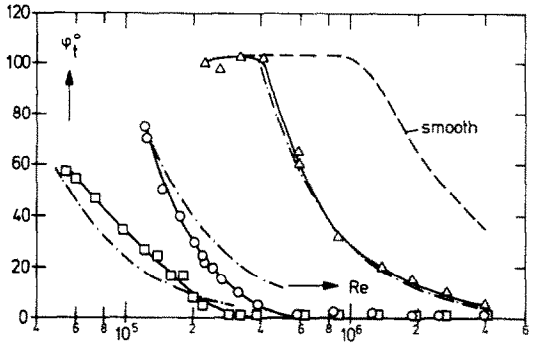

FIG. 27. Transition point from laminar to turbulent boundary layer as a function of Re and roughness parameter k_s/d. Symbols as in Fig. 8; —.—.—, equation (6).

φ_t, as a function of the Reynolds number. The surface roughness occurs as a parameter. It is seen that with increasing Reynolds number the transition point moves towards the front stagnation point. At a fixed point on the cylinder the boundary layer undergoes transition from laminar to turbulent flow with increasing roughness parameter at lower Reynolds numbers. This evidence can be described by equation (6) (dashed-dotted lines in Fig. 27):

$$\varphi_t = \frac{1.63 \times 10^5}{(Re\, k_s/d)^{1.3}}. \qquad (6)$$

Equation (6) is an empirical formula obtained by a best fit line through the experimental points. It is surprising that the phenomenon can roughly be described by the parameter $(Re\, k_s/d)$, which is a Reynolds number formed with the roughness height k_s and the undisturbed velocity U_∞.

Final remarks

The tests were intended to be carried out at the boundary condition T_w = constant. However, at the highest Reynolds number the variation of the local heat-transfer coefficient around the cylinder caused a deviation of the local temperature from the mean value by about $\pm 15\%$. Comparing this experimental value with that predicted according to the formula given in [1], a good agreement is found: the theory yields a value of $\pm 14.8\%$.

At lower Reynolds numbers ($Re < 3 \times 10^5$) the heat transferred by radiation cannot be neglected in comparison with the total heat transfer. It was assumed that for each of the rough surfaces the emission constant was equal to $\varepsilon = 0.4$. Tests are being conducted to determine experimentally the exact value.

For the evaluation of the local heat-transfer data it was assumed that half the thickness of the thermal insulation separating the copper plug from its surroundings contribute to the heat transfer. The temperature distribution at the surface of the insulation was calculated according to the analysis described in [6]: this correction becomes substantial particularly at high Reynolds numbers.

Acknowledgements—The tests were carried out in the laboratories of the "Institut für Reaktorbauelemente, Kernforschungsanlage Jülich GmbH". The Director of the Institute, Prof. von der Decken, to whom the author is very grateful, supported this work with great interest. The author is also indebted to his assistants H. Gillessen, F. Hoffmanns, H. Reger and R. Rommerskirchen, who prepared and performed the tests with great care.

REFERENCES

1. E. Achenbach, Total and local heat transfer from a smooth circular cylinder in cross-flow at high Reynolds number, *Int. J. Heat Mass Transfer* **18**, 1387–1396 (1975).
2. A. Fage and J. H. Warsap, The effect of turbulence and surface roughness on the drag of a circular cylinder, Aero. Res. Counc. R. & M. No. 1283 (1930).
3. E. Achenbach, Influence of surface roughness on the cross-flow around a circular cylinder, *J. Fluid Mech.* **46**, 321–335 (1971).
4. E. Achenbach, The effects of surface roughness and tunnel blockage on the flow past spheres, *J. Fluid Mech.* **65**, 113–125 (1974).
5. P. Daujotas, J. Žiugžda and A. Žukauskas, Heat transfer of a single cylinder in cross-flow of water at critical Reynolds number, *Dokl. Akad. Nauk. Lith. SSR* Ser. B **3**(76), 99–109 (1973) (Russian).
6. E. Achenbach and N. Iniotakis, Analytische Behandlung der zweidimensionalen Wärmeleitung in einem Rechteckquerschnitt bei vorgegebenen Randbedingungen, KFA-Bericht Jül-1172 (1975).

EFFET DE LA RUGOSITE SUPERFICIELLE D'UN CYLINDRE CIRCULAIRE SUR LE TRANSFERT THERMIQUE POUR UN ECOULEMENT D'AIR TRANSVERSAL

Résumé—On a étudié l'influence de la rugosité superficielle d'un cylindre circulaire sur le transfert thermique pour un écoulement transversal. Le nombre de Reynolds varie de $2{,}2 \times 10^4$ à 4×10^6. La variation du paramètre de rugosité est $0 < k_s/d < 900 \times 10^{-5}$. Les essais correspondent à la condition à la limite T constante.

On a mesuré pour chacun des cylindres rugueux la répartition de pression statique et les transferts thermiques locaux et globaux. Une attention particulière a été portée sur la transition laminaire—turbulent de la couche limite en fonction du nombre de Reynolds et du paramètre de rugosité.

DER EINFLUSS DER OBERFLÄCHENRAUHIGKEIT AUF DEN WÄRMEÜBERGANG BEI EINEM MIT LUFT QUER ANGESTRÖMTEN KREISZYLINDER

Zusammenfassung—Der Einfluß der Oberflächenrauhigkeit auf den Wärmeübergang beim querangeströmten Kreiszylinder wurde untersucht. Die Versuche wurden in Luft unter atmosphärischen Bedingungen sowie in einem Hochdruck-Gaskanal durchgeführt. Dadurch konnte die Reynolds–Zahl im Bereich $2.2 \times 10^4 < Re < 4 \times 10^6$ variiert werden. Die Variation des Rauhigkeitsparameters betrug $0 < k_s/d < 900 \times 10^{-5}$. Den Experimenten lag die Randbedingung $T \approx$ const. zugrunde.

Für jede der Rauhigkeiten wurden die Verteilung des statischen Druckes sowie der örtliche und integrale Wärmeübergang bestimmt. Weiterhin wurde der Umschlag laminar–turbulent als Funktion der Reynolds–Zahl und des Rauhigkeitsparameters experimentell ermittelt.

ВЛИЯНИЕ ШЕРОХОВАТОСТИ НА ТЕПЛООБМЕН КРУГЛОГО ЦИЛИНДРА, ОБТЕКАЕМОГО ПОПЕРЕЧНЫМ ПОТОКОМ ВОЗДУХА

Аннотация — Проведено исследование влияния шероховатости поверхности на теплообмен круглого цилиндра, обтекаемого поперечным потоком воздуха при граничном условии $T \approx$ const в диапазоне изменения числа Рейнольдса $2{,}2 \times 10^4$–4×10^6 и параметра шероховатости $0 < k_s/D < 900 \times 10^5$. Для каждого из цилиндров, имеющих шероховатую поверхность, измерялись распределение статического давления, а также локальные и общие коэффициенты теплообмена. Особое внимание обращалось на влияние числа Рейнольдса и параметра шероховатости на переход от ламинарного пограничного слоя к турбулентному.